

# Optical Integrated Sensing and Communication

Runxin Zhang<sup>†</sup>, Yulin Shao<sup>§</sup>, *Member, IEEE*, Menghan Li<sup>†</sup>, Lu Lu<sup>†</sup>, *Member, IEEE*

<sup>†</sup>University of Chinese Academy of Sciences, Beijing 101408, China

<sup>†</sup>Key Laboratory of Space Utilization, Chinese Academy of Sciences, Beijing 100094, China

<sup>§</sup>Department of Engineering, University of Exeter, Exeter EX4 4PY, United Kingdom

**Abstract**—This paper explores a new paradigm of optical integrated sensing and communication systems (O-ISAC). Our investigation reveals that optical communication and optical sensing are two inherently complementary technologies. On the one hand, optical communication provides the necessary illumination for optical sensing. On the other hand, optical sensing provides environmental information for optical communication. These insights form the foundation of a directionless integrated system, which constitutes the first phase of O-ISAC. We further put forth the concept of optical beamforming using the collimating lens, whereby the light emitted by optical sources is concentrated onto the target device. This greatly improves communication rate and sensing accuracy, thanks to remarkably increased light intensity. Simulation results confirm the significant performance gains of our O-ISAC system over a separated sensing and communication system. With the collimating lens, the light intensity arrived at the target object is increased from 1.09% to 78.06%. The sensing accuracy and communication BER are improved by 62.06 dB and 65.52 dB, respectively.

**Index Terms**—ISAC, optical communication, optical sensing, collimating lens.

## I. INTRODUCTION

With the growing demand of higher communication rates for mobile devices, researchers are exploring new frequency resources and signal processing techniques for next-generation communication systems. A technique that has recently gained significant attention is integrated sensing and communication (ISAC) [1]–[5]. The essence of ISAC is utilizing the time and frequency resources originally allocated to radar, and designing a unified transceiver that achieves wireless communication and remote sensing simultaneously with a single hardware platform [4]–[6].

Existing research efforts on ISAC have mostly been focused on the radio bands. In this paper, we explore the integration of communication and sensing in a much higher frequency band – the optical band.

Optical communication is a wireless communication technology that encodes information by the variations of light intensity, which is known as *intensity modulation*. Compared to radio communication, the optical band is ultra-wide and license-free – it consists of three sub-bands: the infrared (IR), the visible, and the ultraviolet (UV). Therefore, optical communication is viewed as a promising complement to radio communication in next-generation communication systems [7] to address the problem of spectrum scarcity. On the other hand, optical sensing is an estimation technology that measures the presence or absence of objects, distance, displacement, etc.,

with high precision by capturing the intensity of incident light rays and converting it into a form readable by a measuring device.

As will be revealed in the main body of this paper, optical communication and sensing are complementary to each other in nature. Specifically,

- **Optical communication provides the necessary illumination for optical sensing.**

Optical sensing requires light sources, such as LEDs, infrared radiators, and lasers. The light emitted by an optical communication transmitter can be naturally collected and utilized for optical sensing. Importantly, optical sensing relies only on the intensity of the incident light, hence the optical communication waveforms do not need to be redesigned to optimize the sensing accuracy. This is different from the ISAC operated on the radio band, where the waveforms of the ISAC transmitter have to be carefully designed to accommodate both communication and sensing, resulting in a trade-off between communication rate and sensing accuracy (that is, ISAC reaps the communication rate gains by compromising the sensing accuracy).

- **Optical sensing provides the environmental information to optical communication.**

The performance of optical communication can be greatly improved when accurate environmental parameters are given, e.g., the orientation of targets, the environment map, the distance to the receiver, etc. These parameters can be provided by optical sensing and benefits optical communication.

In the above light, this paper envisions and develops an optical integrated communication and sensing (O-ISAC) system. Our main contributions are summarized as follows.

- 1) We put forth the concept of O-ISAC and develop the first O-ISAC system with two operational phases. The first phase is directionless O-ISAC, wherein optical access points (AP) broadcast directionless light for communication, and sense the environment based on the reflected light. The second phase is directional O-ISAC, where the optical APs transmit directional light to serve users, thereby enhancing the light intensity for both optical communication and sensing.
- 2) To realize the directional O-ISAC in the second phase, we coin a new concept of optical beamforming, leveraging the collimating lens. The profile of the collimating lens surface is characterized analytically. By taking the

frequency dispersion of optical sources into account, we establish a decent approximation of the divergence angle of different wavelength components of the optical source when passing through the lens.

- 3) Simulation results validate the superior performance of our O-ISAC system. Compared to the system where sensing and communication are performed separately, directionless O-ISAC in the first phase improves the sensing accuracy and communication bit error rate (BER) by 3.76 dB and 3.01 dB, respectively. In the second phase, optical beamforming greatly concentrates the light, bringing significant performance gains over the separated system. Specifically, with the collimating lens, the light intensity arrived at the target object is increased from 1.09% to 78.06%. The sensing accuracy and communication bit error rate (BER) is improved by 62.06 dB and 65.52 dB, respectively.

**Related work:** Existing research on ISAC is devoted to the optimization of beamforming [8]–[11], waveform design [12]–[14], PAPR [15], security [16], and so on. ISAC has also been combined with other technologies, such as intelligent reflecting surfaces [17]–[20], edge intelligence [21], 5G New Radio [22], reconfigurable holographic surface [23], Unmanned Aerial Vehicle [24]–[27].

Two papers that are more relevant to our paper are [28] and [29], where the authors extend ISAC to the THz band. A solution of the virtual aperture is proposed in [28] with multiple chains to justify the capability of high-resolution THz sensing on portable communication devices. Ref. [29] reveals the potential of bringing forth ISAC and THz transmission together by examining technologies such as antenna and array design, hybrid beamforming, etc.

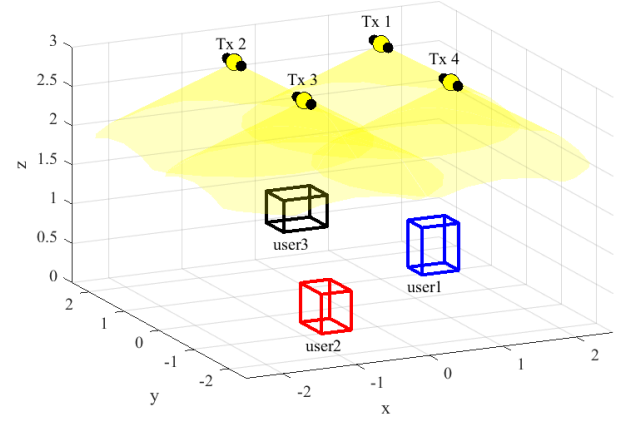
**Notations:** We use boldface lowercase letters to denote column vectors (e.g.,  $\mathbf{x}$ ,  $\mathbf{v}$ ) and boldface uppercase letters to denote matrices (e.g.,  $\mathbf{\tilde{X}}$ ,  $\mathbf{S}$ ). For a vector or matrix,  $(\cdot)_{(a,b)}$  denotes the elements of row  $a$  and column  $b$ ,  $(\cdot)^\top$  denotes the transpose, and  $(\cdot)^H$  denotes the conjugate transpose.  $\mathbb{R}$  and  $\mathbb{C}$  stand for the sets of real and complex values, respectively.  $c$  represents the speed of light, and  $m_0$  is Lambert's mode number. The vectorization function and de-vectorization function are denoted by  $\text{vec}(\cdot)$  and  $\text{devec}(\cdot)$ ,  $(\cdot) \otimes (\cdot)$  denotes the Kronecker product,  $\delta(\cdot)$  denotes the Dirac delta function, and  $\text{diag}\{\cdot\}$  represents diagonal matrix.

## II. OVERVIEW

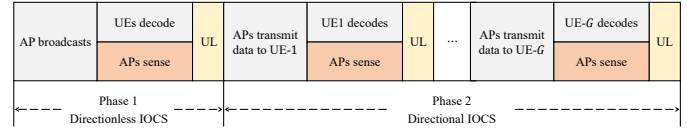
This section overviews the system model and operation flow of the proposed O-ISAC framework. We consider an indoor optical system with  $M$  distributed optical access points (APs), where each AP is equipped with an LED (light source) and a pair of pinhole cameras (optical sensor), as shown in Fig. 1(a). Let there be  $G$  devices and each device is equipped with a PD as the optical receiver.

The proposed O-ISAC framework consists of two alternating phases, the workflows of which are illustrated in Fig. 1(b).

- **Phase 1** (directionless O-ISAC): The APs broadcast a control message to all devices periodically in Phase 1, and



(a) System setup



(b) Workflow

Fig. 1: System model of the proposed O-ISAC system: (a) system setup; (b) workflows of O-ISAC, the two phases alternate with each other.

sense the devices' states globally based on the reflected light.

- **Phase 2** (directional O-ISAC): The APs serve the devices in a TDMA fashion. Given the sensed states in the first phase, the communications between the APs and devices are improved by *optical beamforming*, which we will detail later in Section IV. The APs further utilize the reflected light of phase 2 to accurately sense and track the devices' states.

The detailed operations and signal processing in the two phases are presented in Sections III and IV.

## III. PHASE 1: DIRECTIONLESS O-ISAC

Unlike radio communication, phase modulation and coherent detection in optical communication are very expensive to realize, as it is challenging to match the frequency and polarization of the local laser with that of the incoming optical signal, or even impossible due to the incoherent light emitted by LED [30]. The modulation and demodulation schemes that find wide applications in optical communication systems are intensity modulation and direct detection (IM/DD). In this section, we shall formulate the downlink communications and sensing between the APs and devices in the first phase.

### A. Optical communication

Consider an OFDM-enabled O-ISAC system with  $N$  orthogonal subcarriers. Let  $\mathbf{U} = [\mathbf{u}_1, \mathbf{u}_2, \dots, \mathbf{u}_L] \in \mathbb{C}^{(N/2-1) \times L}$  be a matrix of  $(N/2 - 1) \times L$  complex symbols to be transmitted to the devices. For intensity modulation, we impose the Hermitian symmetry constraint [31] on the input of inverse discrete Fourier transform (IDFT) to perform OFDM modulation.

That is, we construct a matrix  $\mathbf{X} = [\mathbf{x}_1, \mathbf{x}_2, \dots, \mathbf{x}_L] \in \mathbb{C}^{N \times L}$ , where

$$\mathbf{x}_\ell = [0, u_{\ell,1}, u_{\ell,2}, \dots, u_{\ell,N/2-1}, 0, u_{\ell,N/2-1}^*, \dots, u_{\ell,2}^*, u_{\ell,1}^*]^\top, \quad (1)$$

$\ell = 1, 2, \dots, L$ , and perform an  $N$ -point IDFT to obtain IM/DD-compatible real-valued OFDM samples  $\mathbf{V} \in \mathbb{R}^{N \times L}$ .

Recall that we use lowercase bold letters to represent the column-wise vectorized form of a matrix, e.g.,  $\mathbf{x} \triangleq \text{vec}(\mathbf{X})$  and  $\mathbf{v} \triangleq \text{vec}(\mathbf{V})$ . The transformation from  $\mathbf{x}$  to  $\mathbf{v}$  can be expressed as

$$\mathbf{v} = (\mathbf{I}_L \otimes \mathbf{F}_N^H) \mathbf{x}, \quad (2)$$

where  $\mathbf{F}_N$  denotes the  $N$ -point discrete Fourier transform (DFT) matrix (hence  $\mathbf{F}_N^H$  is the IDFT matrix);  $\otimes$  denotes the Kronecker product;  $\mathbf{I}_L$  denotes the  $L$ -dimensional identity matrix.

The real symbols  $\mathbf{v}$  are then assigned to the APs, yielding a transmission matrix  $\mathbf{S} \in \mathbb{R}^{NL \times M}$ :

$$\mathbf{S} = \mathbf{1}_M^\top \otimes \mathbf{v}, \quad (3)$$

where  $\mathbf{1}_M$  represents an all-ones vector of length  $M$ .

Without loss of generality, we consider one device in the system. The received signal of size  $NL \times 1$  can be written as<sup>1</sup>

$$\mathbf{r} = \mathbf{S} \Delta \mathbf{h} + \mathbf{w}, \quad (4)$$

where  $\mathbf{h} = [h_1, h_2, \dots, h_M]^\top$  is the channel coefficient vector;  $\Delta = \text{diag}\left\{\delta\left(t - \frac{d_1}{c}\right), \delta\left(t - \frac{d_2}{c}\right), \dots, \delta\left(t - \frac{d_M}{c}\right)\right\}$  is a delay matrix, in which  $d_m$  denotes the distance between the  $m$ -th AP and the device;  $\mathbf{w} \in \mathbb{C}^{NL \times 1}$  is additive white Gaussian noise (AWGN) added to the electrical domain signal [33].

LED is often modelled as a Lambertian source. For the light emitted by the  $m$ -th AP, the radiation intensity at the device surface  $I_m^{\text{rx}}$  can be written as a function of the transmission intensity  $I_m^{\text{tx}}$ :

$$I_m^{\text{rx}} = I_m^{\text{tx}} \cdot R(\alpha_m) \cdot \Omega_m \cdot g \cdot T_s, \quad (5)$$

where

- 1)  $0 \leq \alpha_m \leq \Phi_{1/2}$  and  $0 \leq \psi_m \leq \Psi_{FOV}$  are the emission angle and incident angle, respectively;  $\Phi_{1/2}$  denotes the LED semi-angle at half power;  $\Psi_{FOV}$  denotes the half-angle field-of-view (FOV) of the PD;
- 2)  $R(\theta_m) = \frac{m_0+1}{2\pi} \cos^{m_0}(\theta_m)$  is the distribution of generalized Lambertian radiant intensity with Lambert's mode number  $m_0 = -\frac{1}{\log_2(\cos \Phi_{1/2})}$  [34];
- 3)  $\Omega_m = \frac{A_{\text{PD}} \cos(\psi_m)}{d_m^2}$  is the solid angle, in which  $A_{\text{PD}}$  is the PD area (hence  $A_{\text{PD}} \cos(\psi_k)$  is the effective detection area);
- 4)  $g$  and  $T_s$  are the gains of a non-imaging concentrator and an optical bandpass filter, respectively. Both can be treated as constants.

<sup>1</sup>In optical communication, the reflected signal can be omitted when the direct signal and the reflected signal co-exist, as the amplitude of the reflected light is much smaller than that of the direct signal [32]. In other words, optical communication links can be treated as direct line of sight (LoS) links.

Then, the channel gain between the  $m$ -th AP and the device can be represented as

$$h_m = \frac{I_m^{\text{rx}}}{I_m^{\text{tx}}} = g T_s \frac{(m_0+1) A_{\text{PD}}}{2\pi d_m^2} \cdot \cos^{m_0}(\alpha_m) \cos(\psi_m). \quad (6)$$

Given the received signal in (4), the device performs DFT and obtains

$$\mathbf{y} = (\mathbf{F}_N \otimes \mathbf{I}_L) \mathbf{r}. \quad (7)$$

Note that  $\mathbf{y} \in \mathbb{C}^{NL \times 1}$  and its matrix form  $\mathbf{Y} = \text{devec}(\mathbf{y}) \in \mathbb{C}^{N \times L}$ . In particular, the element on the  $n$ -th row and  $\ell$ -th column of  $\mathbf{Y}$  is given by

$$\mathbf{Y}_{(n,\ell)} = \sum_{m=1}^M \left[ H_m e^{-j2\pi \frac{n}{N} \frac{d_m}{c}} \mathbf{X}_{(n,\ell)} \right] + \mathbf{w}_{(n,\ell)}, \quad (8)$$

where  $\mathbf{w} = \text{devec}(\mathbf{W})$ . We can then get an estimate of  $\mathbf{X}$  via maximum likelihood estimation, yielding

$$\widehat{\mathbf{X}}_{(n,\ell)} = \arg \max_{\mathbf{X}_{(n,\ell)}} \Pr \{ \mathbf{Y}_{(n,\ell)} | \mathbf{X}_{(n,\ell)} \}. \quad (9)$$

The transmitted message can be reconstructed as

$$\widehat{\mathbf{U}}_{(n,\ell)} = \frac{1}{2} \left( \widehat{\mathbf{X}}_{(n+1,\ell)} + \widehat{\mathbf{X}}_{(N+1-n,\ell)}^* \right). \quad (10)$$

## B. Optical sensing

Optical sensing aims to detect and measure various physical, chemical, or biological parameters, such as position, temperature, pressure, medical diagnostics, etc. In this paper, we focus on positional sensing to estimate the three-dimensional (3D) coordinate of the target device.

Suppose the real-world 3D coordinate of the target device is  $\mathbf{p}_W = (x_W, y_W, z_W)$ . We consider one AP and index the two pinhole cameras by  $i = 1, 2$ . Each pinhole camera maintains a camera coordinate system, in which the pinhole is the origin with the coordinate  $(0, 0, 0)$ . The relative position of one camera to another is fixed, hence we can design the two camera coordinate systems such that they share the same orientation (i.e., the directions of  $x$ ,  $y$ , and  $z$  axes). In this way, if we denote by  $\mathbf{p}_{C,i} = (x_{C,i}, y_{C,i}, z_{C,i})$  the 3D coordinate of the target device in the  $i$ -th camera coordinate system, we have  $x_{C,1} = x_{C,2} \triangleq x_C$ ,  $y_{C,1} = y_{C,2} + v$ , and  $z_{C,1} = z_{C,2} \triangleq z_C$ , where  $v$  is the distance between the two pinholes. Moreover, the camera coordinate system and the world coordinate can be converted to each other via

$$\begin{bmatrix} \mathbf{p}_{C,i} \\ 1 \end{bmatrix} = \begin{bmatrix} \mathbf{Q}_i & \mathbf{t}_i \\ 0 & 1 \end{bmatrix} \begin{bmatrix} \mathbf{p}_W \\ 1 \end{bmatrix}, \quad i = 1, 2, \quad (11)$$

where  $\{\mathbf{Q}_i : i = 1, 2\}$  are  $3 \times 3$  rotation matrices and  $\{\mathbf{t}_i : i = 1, 2\}$  are  $3 \times 1$  positional vectors.

In ISAC with radio communication [6], people often assume that there exists only a finite number of scatters in the environment, hence the number of echoes is small. In contrast, this paper considers a more realistic setup, where all objects in the environment can be reflectors and the reflected light from all range bins of the environment will be collected by the

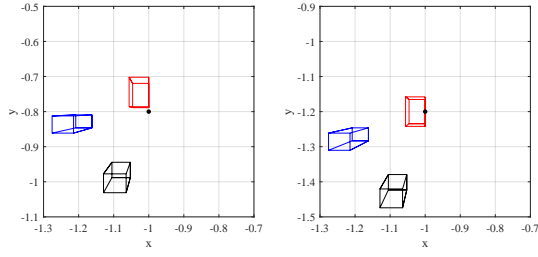


Fig. 2: An illustration of the film planes captured by the two pinhole cameras of an optical AP.

optical sensor. Specifically, at the AP, each pinhole camera maps all reflected light onto a film plane. An illustration is given in Fig. 2, in which the pinhole cameras of the AP capture two images of the environment from two angles.

Each film plane has a 2D plane coordinate system. We denote by  $\mathbf{p}_i = (x_i, y_i)$  the coordinate of the target device on the 2D plane coordinate systems. According to the pinhole imaging principle,  $\mathbf{p}_i$  can be obtained from either  $\mathbf{p}_{C,i}$  or  $\mathbf{p}_W$ . Their relationships can be written as

$$z_{C,i} \begin{bmatrix} \mathbf{p}_i \\ 1 \end{bmatrix} = \begin{bmatrix} f_{x,i} & 0 & 0 \\ 0 & f_{y,i} & 0 \\ 0 & 0 & 1 \end{bmatrix} \mathbf{p}_{C,i} = \mathbf{K}_i [\mathbf{Q}_i \quad \mathbf{t}_i] \begin{bmatrix} \mathbf{p}_W \\ 1 \end{bmatrix}, \quad (12)$$

where  $f_{x,p}$  and  $f_{y,p}$  are interior parameters (focal lengths) of the pinhole camera and  $\mathbf{K}_i \triangleq \begin{bmatrix} f_{x,i} & 0 & 0 \\ 0 & f_{y,i} & 0 \\ 0 & 0 & 1 \end{bmatrix}$  denotes the interior orientation parameters (IOPs); the matrix  $[\mathbf{Q}_i \quad \mathbf{t}_i]$  denotes the exterior orientation parameters (EOPs). In particular, we assume the IOPs of the two cameras are the same and define  $\mathbf{K}_1 = \mathbf{K}_2 \triangleq \mathbf{K}$ .

Given the sensed images, we can perform image processing algorithms to estimate the coordinates of the target. The estimation accuracy depends on the light intensity and the contrast ratio. Since the received light intensity is contaminated by AWGN, we can assume the estimation error of the coordinates follows Gaussian distributions when the pixel size is sufficiently small, and the variance of the estimation error is inversely proportional to the light intensity. That is, the estimated coordinates

$$\hat{\mathbf{p}}_i = \mathbf{p}_i + \mathbf{e}_i = \begin{bmatrix} x_i \\ y_i \end{bmatrix} + \begin{bmatrix} e_{i,x} \\ e_{i,y} \end{bmatrix}, \quad (13)$$

where the estimation error  $e_{i,x}, e_{i,y} \sim \mathcal{N}(0, \eta \frac{\sigma_I^2}{I_{\text{ref}}})$ ;  $\eta$  is a scaling factor determined by the related size of the film plane to the environment and the distance of the film plane to the pinhole;  $\sigma_I^2$  is the variance of AWGN in the received light, and  $I_{\text{ref}}$  is the sensed light intensity given by

$$I_{\text{ref}} = \sum_{m=1}^M \left[ I_m^{\text{tx}} R(\alpha_m) \frac{\cos(\psi_m)}{d_m^2} \right] \cdot \rho_{\text{ref}} A_{\text{ref}} \frac{\cos(\phi_{\text{ref}})}{d_{\text{ref}}^2}. \quad (14)$$

In (14), the first term (i.e., the summation) represents the superposition of the intensities of all light sources on the

reflector,  $\rho_{\text{ref}}$  is the reflection coefficient of the reflector,  $A_{\text{ref}}$  is the reflection area corresponding to the pixel,  $\phi_{\text{ref}}$  is the angle of incidence of the reflected signal, and  $d_{\text{ref},i}$  is the distance between the reflector and the film plane.

To solve  $\mathbf{p}_{C,i}$ , we have

$$\begin{cases} z_C \begin{bmatrix} \hat{\mathbf{p}}_1 \\ 1 \end{bmatrix} = \mathbf{K} \mathbf{p}_{C,1} + \begin{bmatrix} \mathbf{e}_1 \\ 1 \end{bmatrix} \\ z_C \begin{bmatrix} \hat{\mathbf{p}}_2 \\ 1 \end{bmatrix} = \mathbf{K} \mathbf{p}_{C,2} + \begin{bmatrix} \mathbf{e}_2 \\ 1 \end{bmatrix} \end{cases}, \quad (15)$$

After some manipulations, (15) can be reorganized as

$$\begin{bmatrix} 0 \\ -f_y v \\ 0 \\ 0 \end{bmatrix} = \begin{bmatrix} f_x & 0 & -\hat{x}_1 \\ 0 & f_y & -\hat{y}_1 \\ f_x & 0 & -\hat{x}_2 \\ 0 & f_y & -\hat{y}_2 \end{bmatrix} \begin{bmatrix} x_C \\ y_{C,2} \\ z_C \end{bmatrix} + \begin{bmatrix} e_{1,x} \\ e_{1,y} \\ e_{2,x} \\ e_{2,y} \end{bmatrix} \quad (16)$$

$$\triangleq \boldsymbol{\gamma} = \boldsymbol{\Sigma} \mathbf{p}_{C,i} + \boldsymbol{\epsilon},$$

from which  $\hat{\mathbf{p}}_{C,2}$  can be estimated by

$$\hat{\mathbf{p}}_{C,2} = (\boldsymbol{\Sigma}^\top \boldsymbol{\Sigma})^{-1} \boldsymbol{\Sigma}^\top \boldsymbol{\gamma}^\top, \quad (17)$$

$$\hat{\mathbf{p}}_{C,1} = \hat{\mathbf{p}}_{C,2} + [0, v, 0]^\top. \quad (18)$$

Finally, the 3D coordinates of the target device in the world coordinate system can be calculated from (11) as

$$\begin{bmatrix} \hat{\mathbf{p}}_W \\ 1 \end{bmatrix} = \begin{bmatrix} \mathbf{Q}_i & \mathbf{t}_i \\ 0 & 1 \end{bmatrix}^{-1} \begin{bmatrix} \hat{\mathbf{p}}_{C,i} \\ 1 \end{bmatrix}. \quad (19)$$

We use the mean-squared error (MSE) of the coordinates to measure the sensing accuracy. That is,

$$\text{MSE}_P = \mathbb{E} \left\{ \|\hat{\mathbf{p}}_W - \mathbf{p}_W\|^2 \right\}. \quad (20)$$

This section focuses on the sensing operation at a single AP. More generally, multiple APs can collaborate to obtain a more accurate estimation of the coordinates.

#### IV. PHASE 2: DIRECTIONAL O-ISAC

In the first phase of O-ISAC, the APs broadcast control messages to devices and sense the devices' state with the reflected light. Due to the use of directionless light, the strength of the signal received at the devices is low – as a consequence, the communication rate and sensing accuracy of phase 1 are rather limited. In radio communication, an efficient scheme to address such a problem is beamforming, which uses antenna arrays to direct the signal toward specific angles. In optical communication, however, beamforming cannot be realized due to the uncontrollable phase of light.

To achieve spatial selectivity, this paper puts forth the concept of *optical beamforming* for O-ISAC, leveraging the collimating lens. With optical beamforming, the light emitted by APs is directed to the target device, enhancing both the optical communication rate and the sensing accuracy (thanks to the stronger reflected light).

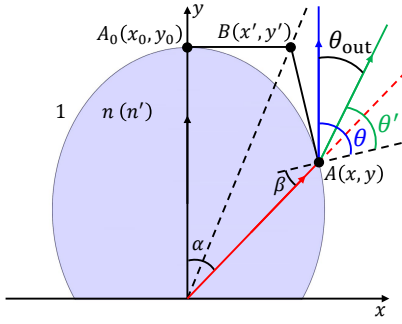


Fig. 3: The cross-section of a collimating lens, where the light emitted from the original is directed to the normal direction of the collimating lens (i.e., the positive direction of the  $y$ -axis).

#### A. Collimating lens

The light intensity becomes lower and lower as it travels, due to the divergence angle  $\alpha_m$  in (6). The collimating lens is a class of curved optical lenses that aligns light in a parallel fashion, thereby preventing the constant diffusion of light. Inspired by this, we can leverage the collimating lens to direct the emitted light to the target receiver, achieving the effect of optical beamforming.

Fig. 3 illustrates the cross-section of a collimating lens, where the light emitted from the original is directed to the normal direction of the collimating lens (i.e., the positive direction of the  $y$ -axis). Complete surface profile of the lens can be obtained when the cross-section is rotated around the axis of revolution symmetry. The collimating lens changes the distribution of light intensity. Thus, the main effort of this section is to analyze the optical channel gains when the collimating lens is employed.

Given the coordinate system in Fig. 3, we first derive the geometric relationship between the profile of the lens surface and the exit angle through the normal vector.

**Proposition 1** (Profile of the lens surface). *The coordinate of any point  $A$  on the lens surface can be represented by the exit angle  $\alpha$  as*

$$A = \left( \tan \frac{\alpha}{2} + \mu(n(\lambda) \cos \alpha - 1), 1 - \mu n(\lambda) \sin \alpha \right), \quad (21)$$

where  $\alpha$  is the emission angle of LED (see (5)),  $\mu = \frac{\tan \alpha - \tan \frac{\alpha}{2}}{(n(\lambda) \cos \alpha - 1) + n(\lambda) \tan \alpha \sin \alpha}$ , and  $n(\lambda) \propto 1/\lambda$  is the refractive index of the collimating lens for the light of wavelength  $\lambda$ .

*Proof.* See Appendix A. ■

It is worth noting that collimating lenses have a critical refraction angle, meaning that the collimation effect is only effective over a range of exit angles. In particular, the effective range of exit angles is determined by the refractive index. When the refractive index is 1.4, for example, the maximum exit angle is about  $\pi/4$ .

#### B. Frequency dispersion of optical sources

Practical optical sources cannot produce light of a single frequency. As an example, Fig. 4 gives Relative spectrum

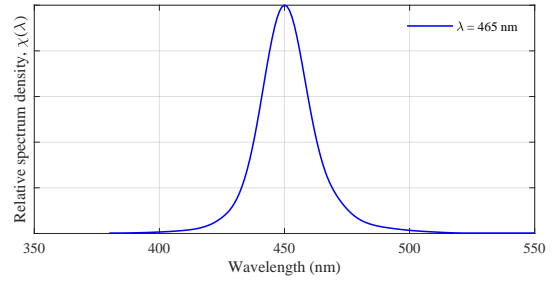


Fig. 4: Illustrating the frequency dispersion effect of a commercial LED: the relative spectrum density as a function of wavelength.

density  $\chi(\lambda)$  of the light emitted by a commercial LED as a function of wavelength. As shown, in addition to the peak wavelength  $\lambda = 465$  nm, the light also contains other wavelengths.

The frequency dispersion phenomenon brings about an important challenge that the collimating lens can only be designed to collimate the light of the peak wavelength. In contrast, other wavelength components cannot be fully collimated and still suffer from a divergence angle. This divergence angle is visualized in Fig. 3. Specifically, we consider the peak wavelength  $\lambda$  and any other wavelength component  $\lambda' \neq \lambda$ . After passing through the lens, we denote by  $\theta$  and  $\theta'$  the emission angle of the lens (w.r.t. the normal of the lens surface) for the light with wavelengths  $\lambda$  and  $\lambda'$ , respectively. Then, the divergence angle  $\theta_{out} = \theta - \theta'$ .

For a given wavelength, accurately characterizing its divergence angle  $\theta_{out}$  is non-trivial. Nevertheless, Proposition 2 establishes a good approximation of  $\theta_{out}$  after a number of manipulations.

**Proposition 2** (The divergence angle). *Consider an optical source and denote the peak wavelength by  $\lambda$ . After passing through the collimating lens, the divergence angle of a wavelength component  $\lambda'$  can be approximated by*

$$\theta_{out} \approx \frac{n(\lambda)}{n(\lambda) - 1} \frac{\lambda' - \lambda}{\lambda'} \alpha. \quad (22)$$

*Proof.* See Appendix B. ■

#### C. O-ISAC with optical beamforming

Given the analysis in the above two sections, we are ready to derive the optical channel gains with collimating lenses.

From (22), we have

$$\alpha(\theta_{out}) \approx \frac{[n(\lambda) - 1]\lambda'}{n(\lambda)(\lambda' - \lambda)} \theta_{out}. \quad (23)$$

For a given wavelength  $\lambda'$ , the portion of the light directed to the PD/reflector over the total light in the downlink communications can be derived as

$$p^{\text{eff}}(\lambda') = \frac{\int_{\tan(\theta_{out}) \cdot d < r} R(\alpha(\theta_{out})) d\theta_{out}}{\int_{\text{all}} R(\alpha(\theta_{out})) d\theta_{out}}$$

$$\begin{aligned}
&= \frac{\int_{\tan(\theta_{\text{out}}) \cdot d < r} \frac{m+1}{2\pi} \cos_0^m(\alpha(\theta_{\text{out}}))}{\int_{\text{all}} \frac{m+1}{2\pi} \cos_0^m(\alpha(\theta_{\text{out}}))} \\
&\stackrel{(a)}{=} \frac{\int_{\tan(\theta_{\text{out}}) \cdot d < r} \cos(\alpha(\theta_{\text{out}})) d\theta_{\text{out}}}{\int_{\text{all}} \cos(\alpha(\theta_{\text{out}})) d\theta_{\text{out}}} \\
&\stackrel{(b)}{=} \frac{\int_{\theta_{\text{out}} \leq \arctan \frac{r}{d}} \cos\left(\frac{[n(\lambda)-1]\lambda'}{n(\lambda)(\lambda'-\lambda)} \theta_{\text{out}}\right)}{\int_{\text{all}} \cos\left(\frac{[n(\lambda)-1]\lambda'}{n(\lambda)(\lambda'-\lambda)} \theta_{\text{out}}\right)} \\
&= \frac{\sin\left(\frac{[n(\lambda)-1]\lambda'}{n(\lambda)(\lambda'-\lambda)} \theta_{\text{out}}\right) \Big|_{\theta_{\text{out,min}}^{\text{eff}}}^{\theta_{\text{out,max}}^{\text{eff}}}}{\sin\left(\frac{[n(\lambda)-1]\lambda'}{n(\lambda)(\lambda'-\lambda)} \theta_{\text{out}}\right) \Big|_{\theta_{\text{out,min}}}} \stackrel{(c)}{=} \frac{\sin\left(\frac{[n(\lambda)-1]\lambda'}{n(\lambda)(\lambda'-\lambda)} \theta_{\text{out,max}}^{\text{eff}}\right)}{\sin\left(\frac{[n(\lambda)-1]\lambda'}{n(\lambda)(\lambda'-\lambda)} \theta_{\text{out,max}}\right)}, \quad (24)
\end{aligned}$$

where  $\theta_{\text{out,max}}^{\text{eff}}$  refers to the maximum divergence angle that can fall onto the PD/reflector, which satisfies  $d \cdot \sin \theta_{\text{out,max}}^{\text{eff}} = r$ ;  $d$  is the distance between the transmitter and receiver/reflector (i.e.,  $d_m$  if we refer to the  $m$ -th AP);  $r$  is the radius of the receiving area (in the case of downlink communication, the receiving area is the area of the PD, hence we have  $A_{PD} = \pi r^2$  in (5));  $\theta_{\text{out,max}}$  is the maximum divergence angle after collimation with  $\theta_{\text{out,max}} \approx \frac{n(\lambda)(\lambda'-\lambda)}{[n(\lambda)-1]\lambda'} \Phi_{1/2}$ .

In the derivation of (24), (a) follows by setting  $m_0 = 1$ , as the typical half-power angle is  $\pi/3$ ; The absolute value symbol can be removed in (b) because  $\cos(\cdot)$  is an even function; (c) follows because  $\theta_{\text{out,min}}^{\text{eff}} = -\theta_{\text{out,max}}^{\text{eff}}$  and  $\theta_{\text{out,min}} = -\theta_{\text{out,max}}$ , thanks to the central symmetry of the light.

Finally, the optical channel gain can be obtained as

$$h^L \triangleq P^{\text{eff}}(\lambda) = \int p^{\text{eff}}(\lambda') \chi(\lambda') d\lambda', \quad (25)$$

where  $\chi(\lambda')$  is the relative spectrum density with  $\int_{\lambda'} \chi(\lambda') d\lambda' = 1$ .

Compared with phase 1, the introduction of collimating lens in the second phase has two main impacts on O-ISAC: For optical communications, the received signal can still be written as (4), but the channel gain is given in (25). For optical sensing, the projection relationship from the environment to the film plane remains unchanged, but the light intensity received by each pixel is

$$I_{\text{ref}} = \sum_{m=1}^M [h_m^L] \cdot \rho_{\text{ref}} A_{\text{ref}} \frac{\cos(\phi_{\text{ref}})}{d_{\text{ref}}^2}, \quad (26)$$

where the optical channel gain from the  $m$ -th AP to the target device  $h_m^L$  is given by (25).

For both communication and sensing, the received light intensity is greatly enhanced with optical beamforming, hence the communication rate and sensing accuracy are remarkably improved.

## V. SIMULATION RESULTS

This section evaluates the proposed O-ISAC system via simulation results. In particular, we shall evaluate both directionless and directional O-ISAC benchmarked against a separated sensing and communication system, in which communication

TABLE I: Parameter settings.

| Parameters        | Description                             | Value                                       |
|-------------------|---|---|
| Environment       | Room dimension                          | $5m \times 5m \times 3m$                    |
| Signal Structure  | No. of bits                             | $6 \times 10^6$                             |
|                   | No. of subcarrier                       | 16  |
|                   | Modulation scheme                       | BPSK-OFDM (phase 1)<br>16QAM-OFDM (phase 2) |
| Source Parameters | No. of LED                              | 4   |
|                   | Source Co-ordinates                     |   |
|                   | LED1                                    | (1m, 1m, 3m)                                |
|                   | LED2                                    | (-1m, 1m, 3m)                               |
|                   | LED3                                    | (-1m, -1m, 3m)                              |
|                   | LED4                                    | (1m, -1m, 3m)                               |
|                   | Semi-half angle of LED ( $\Phi_{1/2}$ ) | $\pi/3$                                     |
|                   | No. of pinholes per Tx.                 | 2   |
|                   | Distance between pinhole and LED        | 0.2 m                                       |
| device Parameters | focal length                            | 0.05 m                                      |
|                   | No. of device                           | 3   |
|                   | No. of PD per device                    | 1   |
|                   | FOV ( $\Psi_{FOV}$ )                    | $\pi/3$                                     |
|                   | Active area of PD ( $A_{PD}$ )          | 1 mm <sup>2</sup>                           |
|                   | Size of convergence lens                | 1 inch                                      |
|                   | Reflection coefficient ( $\rho_j$ )     | 0.8   |

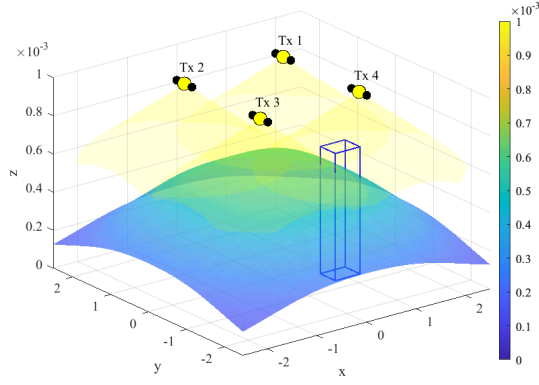
and sensing are independently implemented with half power. The simulation parameters are summarized in Tab. I.

We first simulate the distribution of light intensity in the environment. The directionless O-ISAC and the separated system share the same light intensity distribution, as shown in Fig. 5(a). Specifically,  $M$  APs broadcast signals with semi-angle at half power of  $\Phi_{1/2}$ . The light intensity that falls on the target only accounts for 1.09% of the total light intensity. In phase 2, the collimating lens is used to concentrate the light from APs on the target device. The received light intensity exhibits a distribution shown in Fig. 5(b), where 78.06% of the light intensity falls on the target.

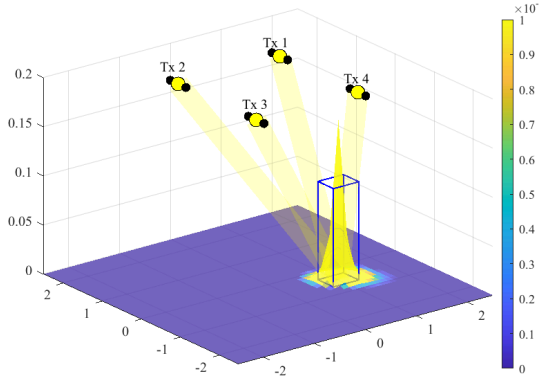
Thanks to the greatly concentrated light intensity, the performances of both optical sensing and communications are improved. Fig. 6 presents the BER performance of the O-ISAC system. As shown, compared with the separated system, directionless O-ISAC exhibits a 3.76 dB gain, while directional O-ISAC exhibits a 65.82 dB gain. Fig. 7 presents the MSE of position estimation in light sensing. Directionless O-ISAC outperforms the separate system by 2.69 dB. Directional O-ISAC, on the other hand, outperforms the directionless system by 58.19 dB.

Overall, in our O-ISAC system, the APs periodically uses a large power (e.g., 90 dB in Fig. 6) to broadcast the control information and sense the devices globally. The BER can be kept to  $10^{-4}$  and the sensing MSE is about 0.035 (this corresponds to a localization accuracy of 20 cm). Then, in the second phase (which is much longer than the first phase), the APs use a relatively low power (e.g., 30 dB in Fig. 6) to serve the users and keep track of the users' locations. The BER performance can be kept below  $10^{-4}$  and the sensing MSE is about  $10^{-2}$  (this corresponds to a localization accuracy within 10 cm).





(a) without collimating lens



(b) with collimating lens

Fig. 5: The distribution of light intensity in the environment, where the blue box represents the position of the target device.

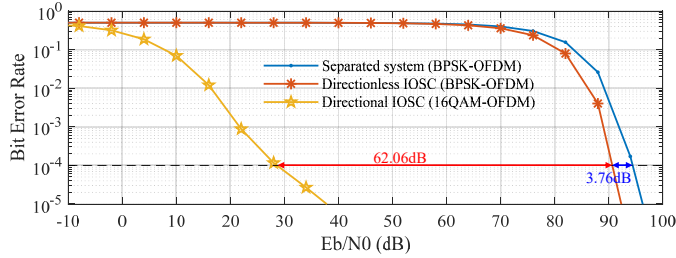


Fig. 6: BER of optical communication with BPSK-OFDM in directionless O-ISAC and 16QAM-OFDM in directional O-ISAC under various  $E_b/N_0$ .

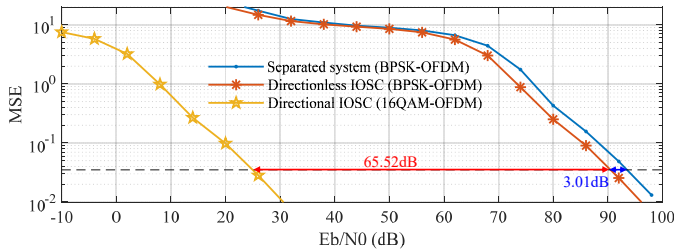


Fig. 7: MSE of position estimation for optical sensing with directionless and directional O-ISAC under various  $E_b/N_0$ .

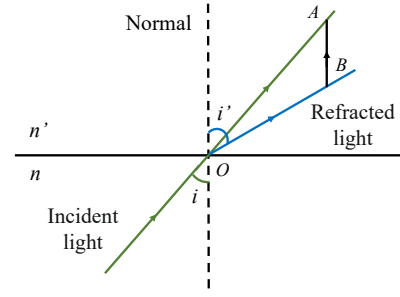


Fig. 8: The vector relationship between the incident light, refracted light, and the surface normal

## VI. CONCLUSION

This paper explored the integration of communication sensing and communication in the optical band. We developed the first optical integrated sensing and communication (O-ISAC) system with two operational phases. The first phase, i.e., the directionless O-ISAC, confirms the feasibility of integrating optical sensing and optical communication. The second phase, i.e., the directional O-ISAC, leverages optical beamforming to significantly enhance the performance of both optical sensing and optical communication. The attempt made in this paper represents a preliminary exploration of O-ISAC. Moving forward, the communication rate and sensing accuracy of O-ISAC can be improved by more advanced techniques, such as the PD array, collaborative sensing, multi-modal sensing, etc.

## APPENDIX A

### PROFILE OF THE LENS SURFACE

This appendix derives the geometric relationship between the profile of the lens surface and the exit angle through the normal vector, based on the coordinate system in Fig. 3.

According to Fermat's principle, we solve the contour of the lens surface through the normal vector. As shown in Fig. 8, the incident light is refracted from the medium with a refractive index of  $n$  through the optical surface into the medium with a refractive index of  $n'$ , which is obtained according to the law of refraction

$$n_1 \sin i_1 = n_2 \sin i_2. \quad (27)$$

The extension of the incident light, the refracted light, and the surface normal form a triangle. According to the law of cosine, we have

$$OA \sin i_1 = OB \sin i_2. \quad (28)$$

Combining (27) and (28) gives us

$$\frac{OB}{OA} = \frac{n_2}{n_1}. \quad (29)$$

Moreover, from the vector relation of  $\triangle OAB$  in Fig. 8, we have

$$\vec{BA} = \vec{OA} - \vec{OB}. \quad (30)$$

The normal vector can be written as

$$\vec{BA} = n_1 \frac{\vec{OA}}{|\vec{OA}|} - n_2 \frac{\vec{OB}}{|\vec{OB}|}. \quad (31)$$

We hope that all the collimated light rays can shoot to the target parallelly, so the exit direction here is the positive direction of the y-axis as shown in Fig. 3, and the incidence direction is the range covered by the semi-half angle of the light source.

With the light source centre being the coordinate origin, we establish a two-dimensional coordinate system. The light direction is parallel to the y-axis after refraction occurs on the surface of the lens. The normal direction is

$$\begin{aligned} \vec{n}_f = \vec{BA} &= (0, 1) \cdot 1 - (\sin \alpha, \cos \alpha) \cdot n \\ &= (-n \sin \alpha, 1 - n \cos \alpha), \end{aligned} \quad (32)$$

where the refractive index of air is 1, and the refractive index of the lens is  $n$ .

Take the red light in Fig. 3 for example, it deflects when passing through point  $A$  on the contour. Draw the tangents at point  $A$  and  $A_0$  respectively, and they intersect at point  $B$ , which is the angular bisector of  $\angle A_0OA$ . The coordinates of point  $B$  is known, and then the coordinates of point  $A$ , which is the contour point we want, can be obtained by draw the perpendicular of the normal at point  $B$ . The perpendicular vector of the normal is

$$\vec{n}'_{f,\perp} = \begin{bmatrix} 0 & -1 \\ 1 & 0 \end{bmatrix} \vec{n}'_f = (n \cos \alpha - 1, -n \sin \alpha). \quad (33)$$

So for the coordinates of point  $A$ , there is

$$\begin{cases} A = B + \mu \cdot \vec{n}'_{f,\perp} \\ \frac{A(x)}{A(y)} = \tan \alpha \end{cases}. \quad (34)$$

That is

$$\frac{\tan \frac{\alpha}{2} + \mu(n \cos \alpha - 1)}{1 - \mu n \sin \alpha} = \tan \alpha \quad (35)$$

Then we can get the relationship between the coordinates of the contour point and the exit angle

$$A = \left( \tan \frac{\alpha}{2} + \mu(n \cos \alpha - 1), 1 - \mu n \sin \alpha \right), \quad (36)$$

where  $\mu = \frac{\tan \alpha - \tan \frac{\alpha}{2}}{(n \cos \alpha - 1) + n \tan \alpha \sin \alpha}$ .

## APPENDIX B

### APPROXIMATING THE DIVERGENCE ANGLE

Considering an optical source and denote the peak wavelength by  $\lambda$ , this appendix approximates the divergence angle  $\theta_{out}$  for a given wavelength  $\lambda'$ .

Let the angle of incidence reaching the lens surface be  $\beta$ , which is consistent for every wavelength, as shown in Fig. 3, and the exit angles of the main wavelength and other wavelengths are  $\theta$  and  $\theta'$ . Then we can construct the relationship as:

$$\begin{cases} \sin \beta \cdot n = \sin \theta \cdot 1 \\ \sin \beta \cdot n' = \sin \theta' \cdot 1 \end{cases}. \quad (37)$$

According to the design rules of the collimating lens, the emission direction of the main wavelength is consistent with the y-axis, so the difference between  $\theta'$  and  $\theta$  is the emission angle of the light with the wavelength  $\lambda'$  and is what we require. According to the geometric relationship and mathematical simplification, we can get (see Appen. B)

$$\theta_{out} = \theta' - \theta \approx \frac{n}{n-1} \frac{1-c}{c} |\alpha|, \quad (38)$$

where  $c = \frac{\lambda'}{\lambda}$ .

In Eq. 37,  $\theta' - \theta$  itself is the difference between exit angles of the two wavelengths, and it's also the direction angle between the other wavelengths and the y-axis that needs to be solved. By computing the ratio of Eq. 37 we have

$$\frac{n}{n'} = \frac{\sin \theta}{\sin \theta'}, \quad (39)$$

so there is

$$\begin{aligned} \theta_{out} &= \theta - \theta' \\ &= \arcsin(\sin \beta \cdot n) - \arcsin\left(\frac{n'}{n} \sin \beta \cdot n\right). \end{aligned} \quad (40)$$

Record the emission angle from the LED as  $\alpha$  (note that it should be less than the critical refraction angle) and the medium incident angle as  $\beta$ , which is the angle between the normal direction of the medium  $(n \sin \alpha, n \cos \alpha - 1)$  and the incident angle vector  $(\sin \alpha, \cos \alpha)$ .  $\alpha$  and  $\beta$  are in one-to-one correspondence

$$\begin{aligned} \beta &= \arccos \left[ \frac{n \sin \alpha \sin \alpha + (n \cos \alpha - 1) \cos \alpha}{\sqrt{n^2 \sin^2 \alpha + (n \cos \alpha - 1)^2}} \right] \\ &= \arccos \left[ \frac{n - \cos \alpha}{\sqrt{n^2 - 2n \cos \alpha + 1}} \right]. \end{aligned} \quad (41)$$

Since the  $\theta_{out}$  we want is in the range of  $10 \sim 20^\circ$ , we can perform Taylor expansion for arcsin at point 0. Then

$$\begin{aligned} \theta_{out} &= \arcsin(n \sin \beta) - \arcsin\left(n \frac{\lambda}{\lambda'} \sin \beta\right) \\ &\approx (n \sin \beta) + \frac{1}{6} (n \sin \beta)^3 + \frac{3}{40} (n \sin \beta)^5 \\ &\quad - \left(n \frac{\lambda}{\lambda'} \sin \beta\right) - \frac{1}{6} \left(n \frac{\lambda}{\lambda'} \sin \beta\right)^3 \\ &\quad - \frac{3}{40} \left(n \frac{\lambda}{\lambda'} \sin \beta\right)^5 \\ &= n \frac{\lambda' - \lambda}{\lambda'} \sin \beta + \frac{1}{6} n^3 \frac{\lambda'^3 - \lambda^3}{\lambda'^3} \sin^3 \beta \\ &\quad + \frac{3}{40} n^5 \frac{\lambda'^5 - \lambda^5}{\lambda'^5} \sin^5 \beta. \end{aligned} \quad (42)$$

The  $\beta$  we want is near 0, so arccos needs to be expanded at point 1, as

$$\begin{aligned} \beta &= \arccos \left[ \frac{n - \cos \alpha}{\sqrt{n^2 - 2n \cos \alpha + 1}} \right] \\ &\approx \sqrt{2 \left( 1 - \frac{n - \cos \alpha}{\sqrt{n^2 - 2n \cos \alpha + 1}} \right)} \end{aligned}$$



$$+ \frac{\sqrt{2}}{12} \left( 1 - \frac{n - \cos \alpha}{\sqrt{n^2 - 2n \cos \alpha + 1}} \right)^{\frac{1}{2}} + \frac{3\sqrt{2}}{160} \left( 1 - \frac{n - \cos \alpha}{\sqrt{n^2 - 2n \cos \alpha + 1}} \right)^{\frac{3}{2}}, \quad (43)$$

where

$$\frac{n - (1 - \frac{1}{2}\alpha^2 + \frac{1}{24}\alpha^4)}{\sqrt{n^2 - 2n(1 - \frac{1}{2}\alpha^2 + \frac{1}{24}\alpha^4) + 1}} = \frac{n - 1 + \frac{1}{2}\alpha^2(1 - \frac{1}{12}\alpha^2)}{\sqrt{(n-1)^2 + n\alpha^2(1 - \frac{1}{12}\alpha^2)}}. \quad (44)$$

When  $0 \leq \alpha \leq \frac{\pi}{3}$ ,  $\frac{1}{12}\alpha^2 < 0.1 \ll 1$ ,

$$\frac{n - (1 - \frac{1}{2}\alpha^2 + \frac{1}{24}\alpha^4)}{\sqrt{n^2 - 2n(1 - \frac{1}{2}\alpha^2 + \frac{1}{24}\alpha^4) + 1}} \approx \frac{n - 1 + \frac{1}{2}\alpha^2}{\sqrt{(n-1)^2 + n\alpha^2}} = \sqrt{1 - \frac{\alpha^2(1 - \frac{1}{4}\alpha^2)}{(n-1)^2 + n\alpha^2}} < 1. \quad (45)$$

Also,  $\frac{3\sqrt{2}}{160} \approx 0.0265$ ,  $\frac{\sqrt{2}}{12} \approx 0.1179$ , we can obtain

$$\beta \approx \sqrt{2 \left( 1 - \sqrt{1 - \frac{\alpha^2(1 - \frac{1}{4}\alpha^2)}{(n-1)^2 + n\alpha^2}} \right)}. \quad (46)$$

Focus on the approximation of  $\alpha$  around 0, so  $\frac{1}{4}\alpha^2 \ll 1$ :

$$\beta \approx \sqrt{2 \left( 1 - \sqrt{1 - \frac{\alpha^2}{(n-1)^2 + n\alpha^2}} \right)} < 1. \quad (47)$$

Then perform Taylor expansion, and we have

$$\sqrt{2 \left( 1 - \sqrt{1 - \frac{\alpha^2}{(n-1)^2 + n\alpha^2}} \right)} \approx \sqrt{\frac{\alpha^2}{(n-1)^2}}. \quad (48)$$

At this time,

$$\begin{aligned} \theta_{\text{out}} &\approx n \frac{\lambda' - \lambda}{\lambda'} \sin \beta + \frac{1}{6} n^3 \frac{\lambda'^3 - \lambda^3}{\lambda'^3} \sin^3 \beta \\ &\quad + \frac{3}{40} n^5 \frac{\lambda'^5 - \lambda^5}{\lambda'^5} \sin^5 \beta \\ &= n \left[ 1 - \frac{\lambda}{\lambda'} \right] \sin \beta + \frac{1}{6} n^3 \left[ 1 - \frac{\lambda^3}{\lambda'^3} \right] \sin^3 \beta \\ &\quad + \frac{3}{40} n^5 \left[ 1 - \frac{\lambda^5}{\lambda'^5} \right] \sin^5 \beta \\ &= n \left[ 1 - \frac{\lambda}{\lambda'} \right] \beta + \frac{1}{6} n^3 \left[ 1 - \frac{\lambda}{\lambda'} \right]^3 \beta^3 \\ &\quad + \frac{3}{40} n^5 \left[ 1 - \frac{\lambda}{\lambda'} \right]^5 \beta^5 \\ &\approx \arcsin \left( n \left( \frac{\lambda}{\lambda'} - 1 \right) \sin \beta \right). \end{aligned} \quad (49)$$

When the angle is small, there is  $\sin x = x$ , then we can get the approximate relationship

$$\theta_{\text{out}} \approx n \left( \frac{\lambda}{\lambda'} - 1 \right) \beta \approx n \left( \frac{\lambda}{\lambda'} - 1 \right) \sqrt{\frac{\alpha^2}{(n-1)^2}} \approx \frac{n(\lambda - \lambda')}{(n-1)\lambda'} |\alpha|. \quad (50)$$

The relationship between Eq. (40) and Eq. (50) are given in Fig. 9, respectively. It can be seen that the approximate result is almost error-free within 0.3rad. Since  $0.3 \text{ rad} \approx 17^\circ$ , this is a reasonable approximation.

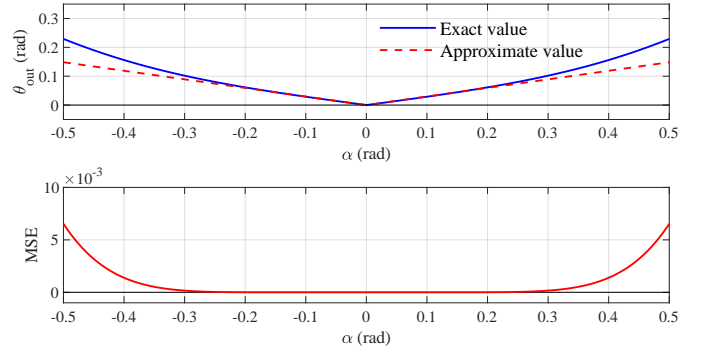


Fig. 9: Approximation of the exit angle after collimation.

## REFERENCES

- [1] D. K. P. Tan, J. He, Y. Li, A. Bayesteh, Y. Chen, P. Zhu, and W. Tong, "Integrated sensing and communication in 6G: motivations, use cases, requirements, challenges and future directions," in *2021 1st IEEE International Online Symposium on Joint Communications & Sensing (JC&S)*, 2021.
- [2] A. Liu, Z. Huang, M. Li, Y. Wan, W. Li, T. X. Han, C. Liu, R. Du, D. K. P. Tan, J. Lu *et al.*, "A survey on fundamental limits of integrated sensing and communication," *IEEE Communications Surveys & Tutorials*, vol. 24, no. 2, pp. 994–1034, 2022.
- [3] F. Liu, Y. Cui, C. Masouros, J. Xu, T. X. Han, Y. C. Eldar, and S. Buzzi, "Integrated sensing and communications: towards dual-functional wireless networks for 6G and beyond," *IEEE journal on selected areas in communications*, 2022.
- [4] Y. Cui, F. Liu, X. Jing, and J. Mu, "Integrating sensing and communications for ubiquitous IoT: applications, trends, and challenges," *IEEE Network*, vol. 35, no. 5, pp. 158–167, 2021.
- [5] Q. Wang, A. Kakkavas, X. Gong, and R. A. Stirling-Gallacher, "Towards integrated sensing and communications for 6G," in *2022 2nd IEEE International Symposium on Joint Communications & Sensing (JC&S)*, 2022.
- [6] F. Liu, C. Masouros, A. P. Petropulu, H. Griffiths, and L. Hanzo, "Joint radar and communication design: applications, state-of-the-art, and the road ahead," *IEEE Transactions on Communications*, vol. 68, no. 6, pp. 3834–3862, 2020.
- [7] E. C. Strinati, S. Barbarossa, J. L. Gonzalez-Jimenez, D. Ktenas, N. Cassiau, L. Maret, and C. Dehos, "6G: The next frontier: From holographic messaging to artificial intelligence using subterahertz and visible light communication," *IEEE Vehicular Technology Magazine*, vol. 14, no. 3, pp. 42–50, 2019.
- [8] H. Hua, J. Xu, and T. X. Han, "Optimal transmit beamforming for integrated sensing and communication," *IEEE Transactions on Vehicular Technology*, 2023.
- [9] M. A. Islam, G. C. Alexandropoulos, and B. Smida, "Integrated sensing and communication with millimeter wave full duplex hybrid beamforming," in *ICC 2022-IEEE International Conference on Communications*, 2022, pp. 4673–4678.
- [10] Z. Xiao and Y. Zeng, "Integrated sensing and communication with delay alignment modulation: performance analysis and beamforming optimization," *IEEE Transactions on Wireless Communications*, 2023.
- [11] C. Qi, W. Ci, J. Zhang, and X. You, "Hybrid beamforming for millimeter wave MIMO integrated sensing and communications," *IEEE Communications Letters*, vol. 26, no. 5, pp. 1136–1140, 2022.
- [12] Z. Xiao and Y. Zeng, "Waveform design and performance analysis for full-duplex integrated sensing and communication," *IEEE Journal on Selected Areas in Communications*, vol. 40, no. 6, pp. 1823–1837, 2022.
- [13] K. Wu, J. A. Zhang, X. Huang, and Y. J. Guo, "Integrating low-complexity and flexible sensing into communication systems," *IEEE Journal on Selected Areas in Communications*, vol. 40, no. 6, pp. 1873–1889, 2022.
- [14] R. Zhang, B. Shim, W. Yuan, M. Di Renzo, X. Dang, and W. Wu, "Integrated sensing and communication waveform design with sparse vector coding: low sidelobes and ultra reliability," *IEEE Transactions on Vehicular Technology*, vol. 71, no. 4, pp. 4489–4494, 2022.

- [15] A. Bazzi and M. Chafii, "On integrated sensing and communication waveforms with tunable PAPR," *IEEE Transactions on Wireless Communications*, 2023.
- [16] O. Günlü, M. R. Bloch, R. F. Schaefer, and A. Yener, "Secure integrated sensing and communication," *arXiv preprint arXiv:2303.11350*, 2023.
- [17] X. Song, D. Zhao, H. Hua, T. X. Han, X. Yang, and J. Xu, "Joint transmit and reflective beamforming for IRS-assisted integrated sensing and communication," in *2022 IEEE Wireless Communications and Networking Conference (WCNC)*, 2022.
- [18] X. Wang, Z. Fei, J. Huang, and H. Yu, "Joint waveform and discrete phase shift design for RIS-assisted integrated sensing and communication system under cramer-rao bound constraint," *IEEE Transactions on Vehicular Technology*, vol. 71, no. 1, pp. 1004–1009, 2021.
- [19] R. Liu, M. Li, H. Luo, Q. Liu, and A. L. Swindlehurst, "Integrated sensing and communication with reconfigurable intelligent surfaces: opportunities, applications, and future directions," *IEEE Wireless Communications*, vol. 30, no. 1, pp. 50–57, 2023.
- [20] X. Wang, Z. Fei, and Q. Wu, "Integrated sensing and communication for RIS assisted backscatter systems," *IEEE Internet of Things Journal*, 2023.
- [21] T. Zhang, S. Wang, G. Li, F. Liu, G. Zhu, and R. Wang, "Accelerating edge intelligence via integrated sensing and communication," in *ICC 2022-IEEE International Conference on Communications*, 2022.
- [22] Y. Cui, X. Jing, and J. Mu, "Integrated sensing and communications via 5G NR waveform: performance analysis," in *ICASSP 2022-2022 IEEE International Conference on Acoustics, Speech and Signal Processing (ICASSP)*, 2022.
- [23] H. Zhang, H. Zhang, B. Di, M. Di Renzo, Z. Han, H. V. Poor, and L. Song, "Holographic integrated sensing and communication," *IEEE Journal on Selected Areas in Communications*, vol. 40, no. 7, pp. 2114–2130, 2022.
- [24] K. Meng, Q. Wu, S. Ma, W. Chen, and T. Q. Quek, "UAV trajectory and beamforming optimization for integrated periodic sensing and communication," *IEEE Wireless Communications Letters*, vol. 11, no. 6, pp. 1211–1215, 2022.
- [25] J. Zhao, F. Gao, W. Jia, W. Yuan, and W. Jin, "Integrated sensing and communications for UAV communications with jittering effect," *IEEE Wireless Communications Letters*, vol. 12, no. 4, pp. 758–762, 2023.
- [26] Z. Lyu, G. Zhu, and J. Xu, "Joint maneuver and beamforming design for uav-enabled integrated sensing and communication," *IEEE Transactions on Wireless Communications*, 2022.
- [27] K. Zhang and C. Shen, "UAV aided integrated sensing and communications," in *2021 IEEE 94th Vehicular Technology Conference (VTC2021-Fall)*, 2021.
- [28] O. Li, J. He, K. Zeng, Z. Yu, X. Du, Y. Liang, G. Wang, Y. Chen, P. Zhu, W. Tong *et al.*, "Integrated sensing and communication in 6G a prototype of high resolution THz sensing on portable device," in *2021 Joint European Conference on Networks and Communications & 6G Summit (EuCNC/6G Summit)*. IEEE, 2021, pp. 544–549.
- [29] A. M. Elbir, K. V. Mishra, S. Chatzinotas, and M. Bennis, "Terahertz-band integrated sensing and communications: challenges and opportunities," *arXiv preprint arXiv:2208.01235*, 2022.
- [30] Z. Wang, Q. Wang, W. Huang, and Z. Xu, *Visible light communications: modulation and signal processing*. John Wiley & Sons, 2017.
- [31] M. Z. Afgani, H. Haas, H. Elgala, and D. Knipp, "Visible light communication using OFDM," in *2nd International Conference on Testbeds and Research Infrastructures for the Development of Networks and Communities*. IEEE, 2006.
- [32] T. Komine and M. Nakagawa, "Fundamental analysis for visible-light communication system using LED lights," *IEEE transactions on Consumer Electronics*, vol. 50, no. 1, pp. 100–107, 2004.
- [33] Z. Ghassemlooy, W. Popoola, and S. Rajbhandari, *Optical wireless communications: system and channel modelling with Matlab®*. CRC press, 2019.
- [34] I. B. Djordjevic, *Advanced optical and wireless communications systems*. Springer, 2018.